Tellus SERIES A DYNAMIC METEOROLOGY AND OCEANOGRAPHY
PUBLISHED BY THE INTERNATIONAL METEOROLOGICAL INSTITUTE IN STOCKHOLM

Tellus (2009), 61A, 227–231
Printed in Singapore. All rights reserved

TELLUS

Transparent lateral boundary conditions for baroclinic waves III. Including vertical shear

By A. MCDONALD*, *Met Éireann, Dublin, Ireland*

(Manuscript received 26 May 2008; in final form 20 August 2008)

ABSTRACT

The problem of how to adapt the so-called transparent boundary conditions to the physical reality that the horizontal advection velocity varies in the vertical, is addressed. A practical demonstration is presented of the transparency of the resulting 'shear' boundary conditions.

1. Introduction

In a previous paper (McDonald, 2005), transparent boundary conditions were derived for the linearized hydrostatic primitive equations in two dimensions. In that paper, a simplifying assumption was made that the advecting velocity did not vary in the vertical. In this paper, that assumption is relaxed and transparent boundary conditions are re-derived for the same set of equations but now allowing for vertical shear in the advection velocity.

2. The hydrostatic equations

In this section, transparent boundary conditions are derived for the two-dimensional linearized hydrostatic primitive equations, including vertical shear in the horizontal advection velocity. A practical demonstration is given of their transparency.

2.1. *The equations of motion*

The linearized inviscid hydrostatic primitive equations in x–z coordinates can be written as follows (See section 8.9 of Gill, 1982, for example).

$$\frac{\partial u'(x,z,t)}{\partial t} + u^0(z)\frac{\partial u'(x,z,t)}{\partial x} + w'(x,z,t)\frac{\mathrm{d}u^0(z)}{\mathrm{d}z} + \frac{1}{\rho^0(z)}\frac{\partial p'(x,z,t)}{\partial x} = 0, \tag{1}$$

$$\frac{\partial \rho'(x,z,t)}{\partial t} + u^0(z)\frac{\partial \rho'(x,z,t)}{\partial x} + \frac{\mathrm{d}\rho^0(z)}{\mathrm{d}z} w'(x,z,t) = 0, \tag{2}$$

$$\frac{\partial p'(x,z,t)}{\partial z} + g\rho'(x,z,t) = 0, \tag{3}$$

$$\frac{\partial u'(x,z,t)}{\partial x} + \frac{\partial w'(x,z,t)}{\partial z} = 0. \tag{4}$$

In these equations the pressure p', the density ρ' and the x- and z-components of the winds u' and w' are small deviations from an isothermal atmosphere, whose fields are designated by the superscript zero and whose density $\rho^0(z)$ and horizontal advective velocity $u^0(z)$ shears in the vertical.

To reduce typographical clutter, define $p = p'$, $\rho = \rho'$, $u = \rho^0 u'$ and $w = \rho^0\, w'$. Then eqs. (1)–(4) become

$$\frac{\partial u(x,z,t)}{\partial t} + u^0(z)\frac{\partial u(x,z,t)}{\partial x} + w(x,z,t)\frac{\mathrm{d}u^0(z)}{\mathrm{d}z} + \frac{\partial p(x,z,t)}{\partial x} = 0, \tag{5}$$

$$\frac{\partial \rho(x,z,t)}{\partial t} + u^0(z)\frac{\partial \rho(x,z,t)}{\partial x} - \frac{N^2}{g}w(x,z,t) = 0, \tag{6}$$

$$\frac{\partial p(x,z,t)}{\partial z} + g\rho(x,z,t) = 0, \tag{7}$$

$$\frac{\partial u(x,z,t)}{\partial x} + \frac{\partial w(x,z,t)}{\partial z} + \frac{N^2}{g}w(x,z,t) = 0, \tag{8}$$

where the Brunt–Väisälä frequency, N^2, is defined in terms of the density as

$$N^2(z) = -\frac{g}{\rho_0(z)}\frac{\mathrm{d}\rho_0(z)}{\mathrm{d}z}. \tag{9}$$

Discretizing in the vertical and defining the ρ and u fields on the 'full' levels and the p and w fields on the 'half' levels gives

*Correspondance
e-mail: aidan.mcdonald@met.ie
DOI: 10.1111/j.1600-0870.2008.00367.x

rise to the following set of equations.

$$\frac{\partial u_m(x,t)}{\partial t} + u_m^0 \frac{\partial u_m(x,t)}{\partial x} + w_m(x,t)\left[\frac{\mathrm{d}u^0(z)}{\mathrm{d}z}\right]_m + \frac{\partial p_m(x,t)}{\partial x} = 0, \quad m = 1, M; \tag{10}$$

$$\frac{\partial \rho_m(x,t)}{\partial t} + u_m^0 \frac{\partial \rho_m(x,t)}{\partial x} - \frac{N^2}{g} w_m(x,t) = 0, \quad m = 2, M; \tag{11}$$

$$\frac{p_{m+\frac{1}{2}}(x,t) - p_{m-\frac{1}{2}}(x,t)}{\Delta z_m} + g\rho_m(x,t) = 0, \quad m = 2, M; \tag{12}$$

$$\frac{p_{\frac{3}{2}}(x,t) - p_{\frac{1}{2}}(x,t)}{\Delta z_1} + g\rho_2(x,t) = 0; \tag{13}$$

$$\frac{\partial u_m(x,t)}{\partial x} + \frac{w_{m+\frac{1}{2}}(x,t) - w_{m-\frac{1}{2}}(x,t)}{\Delta z_m} + \frac{N^2}{g} w_m(x,t) = 0, \quad m = 1, M; \tag{14}$$

where p_m and w_m and Δz_m are defined by

$$p_m \equiv \frac{1}{2}[p_{m+\frac{1}{2}}(x,t) + p_{m-\frac{1}{2}}(x,t)]; \tag{15}$$

$$w_m \equiv \frac{1}{2}[w_{m+\frac{1}{2}}(x,t) + w_{m-\frac{1}{2}}(x,t)]; \tag{16}$$

$$\Delta z_m \equiv z_{m+\frac{1}{2}} - z_{m-\frac{1}{2}}. \tag{17}$$

Finally, it is necessary to define boundary conditions at the 'top' of the atmosphere, $z_{\frac{1}{2}}$, and at the 'bottom' of the atmosphere, $z_{M+\frac{1}{2}}$, where M is the number of full levels. In the absence of orography, the physical boundary condition at the bottom is

$$w_{M+\frac{1}{2}} = 0. \tag{18}$$

At the top of the atmosphere, a material boundary is used to retain the external mode:

$$\frac{\partial p_{\frac{1}{2}}(x,t)}{\partial t} + u_{\frac{1}{2}}^0 \frac{\partial p_{\frac{1}{2}}(x,t)}{\partial x} - g w_{\frac{1}{2}}(x,t) = 0. \tag{19}$$

In the standard Lorenz-grid vertical discretization, eqs. (11) and (12) also hold for $m = 1$, and eq. (13) has ρ_1, not ρ_2. A well-known consequence is that the relationship between the pressure and density is not invertible unless $p_{\frac{1}{2}} = 0$, which contradicts eq. (19); see Section 3.3 of McDonald (2006) for a discussion. Equations (11)–(13) above restore invertibility, which is essential for the present derivation. To proceed, it is necessary to re-formulate eqs. (10)–(19) in matrix format. As a first step, starting from eq. (13), eq. (12) is summed in the vertical with a view to eliminating ρ_m from eq. (11):

$$p_1 = p_{\frac{1}{2}} - g\frac{\Delta z_1}{2}\rho_2,$$

$$p_m = p_{\frac{1}{2}} - g\left[\frac{\Delta z_m}{2}\rho_m + \sum_{j=2}^{m-1}\Delta z_j \rho_j + \Delta z_1 \rho_2\right] \quad m = 2, M. \tag{20}$$

Since there is no ρ_1 in eqs. (10)–(19), that vector element is available to re-name $p_{\frac{1}{2}}$ as

$$p_{\frac{1}{2}} = g\Delta z_1 \rho_1, \tag{21}$$

which when substituted in eq. (20) converts that equation to the matrix form of

$$p_m = \sum_{j=1}^{M} G_{mj}\rho_j; \quad m = 1, M, \tag{22}$$

where G_{mj} is a function of g and Δz_m only. What is important is that this equation can be inverted to express the M values of ρ_m in terms of the M values of p_m:

$$\mathbf{p} = \mathbf{G}\boldsymbol{\rho}; \quad \boldsymbol{\rho} = \mathbf{G}^{-1}\mathbf{p}. \tag{23}$$

The vector field in eq. (21) is not in any sense the density at level 1. It is always $p_{\frac{1}{2}}$ 'in disguise', enabling eq. (19) to be absorbed into the matrix formulation in eq. (26) below. It could equally have been defined via $p_{\frac{1}{2}} = 2g\Delta z_1\rho_1$. This would simply lead to different definition of $\mathbf{G}$.

Summing eq. (14) in the vertical, it can be re-expressed in matrix form as

$$w_m(x,t) = -\frac{g}{N^2}\sum_{j=1}^{M}\tau_{mj}\frac{\partial u_j(x,t)}{\partial x}, \tag{24}$$

$$w_{\frac{1}{2}}(x,t) = -\frac{1}{g}\sum_{j=1}^{M}\nu_j\frac{\partial u_j(x,t)}{\partial x}. \tag{25}$$

The matrix $\boldsymbol{\tau}$ and the transposed vector $\boldsymbol{\nu}$ are functions of Δz, N^2 and g only. Although algebraically complicated, they are rather easy to generate in a computer program because of their recursiveness.

With these definitions, eqs. (19) and (11) can be combined to give the equation

$$\frac{\partial \rho_m(x,t)}{\partial t} + \tilde{u}_m^0\frac{\partial \rho_m(x,t)}{\partial x} + \sum_{j=1}^{M}\tilde{\tau}_{mj}\frac{\partial u_j(x,t)}{\partial x}, \quad m = 1, M; \tag{26}$$

where $\tilde{u}_1^0 = u_{\frac{1}{2}}^0$ and $\tilde{u}_m^0 = u_m^0, m = 2, M$. Also, $\tilde{\tau}_{1j} = \nu_j/(g\Delta z_1)$ and $\tilde{\tau}_{mj} = \tau_{mj}; m = 2, M$.

Equations (10)–(14) and (19) are thus replaced with the following: eqs. (20) and (24), which define $\mathbf{p}$ and $\mathbf{w}$ at the full levels at the start of each time step; eq. (10), which updates $\mathbf{u}$ using both these quantities; and lastly eq. (26), which updates $\boldsymbol{\rho}$. Note that the latter absorbs the upper and lower boundary conditions into the original prognostic equation for $\boldsymbol{\rho}$. Thus, once $\boldsymbol{\rho}$ has been defined initially, the integration can now proceed without needing to compute any field at the 'half levels'. More importantly, the equations are now in a form that lends itself to the derivation of transparent boundary conditions.

2.2. Derivation of the boundary conditions

Using eq. (23) to substitute for ρ_m in eq. (26) yields

$$\frac{\partial p_m(x,t)}{\partial t} + \sum_{l=1}^{M}\sum_{j=1}^{M} G_{ml}\tilde{u}_l^0 G_{lj}^{-1}\frac{\partial p_j(x,t)}{\partial x} + \sum_{l=1}^{M}\sum_{j=1}^{M} G_{ml}\tilde{\tau}_{lj}\frac{\partial u_j(x,t)}{\partial x} = 0. \tag{27}$$

Using eq. (24) to substitute for w_m in eq. (10) yields

$$\frac{\partial u_m(x,t)}{\partial t} + \sum_{j=1}^{M}\left[\delta_{mj}u_j^0 - \frac{g}{N^2}\left(\frac{\mathrm{d}u^0}{\mathrm{d}z}\right)_m \tau_{mj}\right]\frac{\partial u_j(x,t)}{\partial x} + \frac{\partial p_m(x,t)}{\partial x} = 0. \tag{28}$$

The motivation for the inelegant choice of discretization now becomes obvious. Equation (27) requires $\mathbf{G}^{-1}$, which does not exist for the usual Lorenz vertical discretization containing M prognostic equations for density. Equations (28) and (27) can be written as

$$\frac{\partial}{\partial t}\begin{bmatrix}\mathbf{p}\\ \mathbf{u}\end{bmatrix} + \begin{bmatrix}\mathbf{J} & \mathbf{M}\\ \mathbf{I} & \mathbf{K}\end{bmatrix}\frac{\partial}{\partial x}\begin{bmatrix}\mathbf{p}\\ \mathbf{u}\end{bmatrix} = \begin{bmatrix}\mathbf{0}\\ \mathbf{0}\end{bmatrix} \tag{29}$$

where

$$J_{mj} = \sum_{l=1}^{M} G_{ml}\tilde{u}_l^0 G_{lj}^{-1} \tag{30}$$

$$M_{mj} = \sum_{l=1}^{M} G_{ml}\tilde{\tau}_{lj}, \tag{31}$$

$$K_{mj} = \left[\delta_{mj}u_j^0 - \frac{g}{N^2}\left(\frac{du^0}{dz}\right)_m \tau_{mj}\right] \tag{32}$$

and $\mathbf{I}$ is the unit matrix. Defining the $2M$-element vector $\boldsymbol{\Psi}^T = (\mathbf{p}^T, \mathbf{u}^T)$, eq. (29) can be written as

$$\frac{\partial\boldsymbol{\Psi}(x,t)}{\partial t} + \mathbf{A}\frac{\partial\boldsymbol{\Psi}(x,t)}{\partial x} = 0, \tag{33}$$

where $\mathbf{A}$ is the $2M \times 2M$ matrix in eq. (29).

If a matrix $\mathbf{Q}$ exists, which diagonalizes $\mathbf{A}$, then eq. (33) can be re-written as

$$\frac{\partial W_k(x,t)}{\partial t} + \lambda_k\frac{\partial W_k(x,t)}{\partial x} = 0, \tag{34}$$

where

$$\mathbf{W} = \mathbf{Q}^{-1}\Psi \tag{35}$$

and

$$(\mathbf{Q}^{-1}\mathbf{A}\mathbf{Q})_{j,k} = \lambda_k \mathbf{I}_{j,k}, \tag{36}$$

where $\mathbf{I}$ is the $2M \times 2M$-dimensional unit matrix.

Equation (34) describes a plane wave travelling in the $+x$ ($-x$) direction with a velocity $\lambda_i > 0 (< 0)$. To integrate it over a finite non-periodic range, $x = 0$ to L, the field W_k associated with each velocity λ_k pointing into the integration region must be 'imposed' on the boundary from outside. By the same token, to avoid over-specification, the field W_l associated with each velocity λ_l pointing out of the integration region must be 'extrapolated' to the boundary from the integration area, see McDonald (2005). Thus, the boundary wave amplitudes are computed at (0,t) as

$$W_i^r = (\mathbf{Q}^{-1}\boldsymbol{\Psi}^I)_i, \lambda_i > 0; \quad W_i^r = (\mathbf{Q}^{-1}\boldsymbol{\Psi}^E)_i, \lambda_i < 0, \tag{37}$$

and at (L, t) as

$$W_i^r = (\mathbf{Q}^{-1}\boldsymbol{\Psi}^E)_i, \lambda_i > 0; \quad W_i^r = (\mathbf{Q}^{-1}\boldsymbol{\Psi}^I)_i, \lambda_i < 0. \tag{38}$$

Here the superscript I means 'impose' and E means 'extrapolate'. The physical boundary fields themselves are given by

$$\boldsymbol{\Psi}(0,t) = \mathbf{Q}\mathbf{W}^r(0,t); \quad \boldsymbol{\Psi}(L,t) = \mathbf{Q}\mathbf{W}^r(L,t). \tag{39}$$

2.3. Testing the boundary conditions

In this section, a practical demonstration of the transparency of the boundary conditions to outgoing waves is described.

For the time discretization, a leapfrog scheme was used, and for the spatial discretization, the C-grid staggering in the horizontal was used.

For an isothermal atmosphere, $N^2 = g^2/(RT_0)$ with T_0 a constant. The value $T_0 = 250$ K was used; $R = 287.04\,\mathrm{J\,kg^{-1}\,K^{-1}}$. For the discretization, $\Delta x_i = 10$ km, $\Delta t_n = 9.0$ s, $z_{\frac{1}{2}} = 10$ km; $M = 10$ and the levels are equally spaced; thus, $\Delta z_m = -1$ km. The advecting velocity is given a bell-shaped shear, overlaying a background velocity of $10\,\mathrm{m\,s^{-1}}$. The bell is centred at 8000 m and has a half-width of 3000 m and a maximum amplitude of $40\,\mathrm{m\,s^{-1}}$: physically, a strong low-level jet. This results in the following values at the half levels from the top down: $u^0 = (35.6, 45.8, 50.0, 45.8, 35.6, 24.7, 16.8, 12.5, 10.7, 10.2, 10.0)$. These parameters result in the following 20 values of λ_m, in descending order: 310.2, 128.7, 85.5, 68.2, 57.6, 49.7, 43.4, 37.8, 32.4, 27.4, 22.7, 18.1, 13.6, 9.0, 3.8, −2.9, −12.9, −30.9, −72.9, −255.6, all of these having units of $\mathrm{m\,s^{-1}}$. Of these velocities, 15 are greater than and 5 are less than zero.

Two sets of integrations were performed with the same Δx_i and Δt_n; one with $L = 1000$ km, $I = 101$ grid points and a second 'host integration' with $L^h = 10\,000$ km and $I^h = 1001$ grid points. The latter integration was used as the 'correct answer', with which the test integrations were compared.

An initial state, containing all $M = 20$ waves, was constructed as follows, so that each of them has an approximately equal influence on the forecast. Since a pure λ_m wave has all

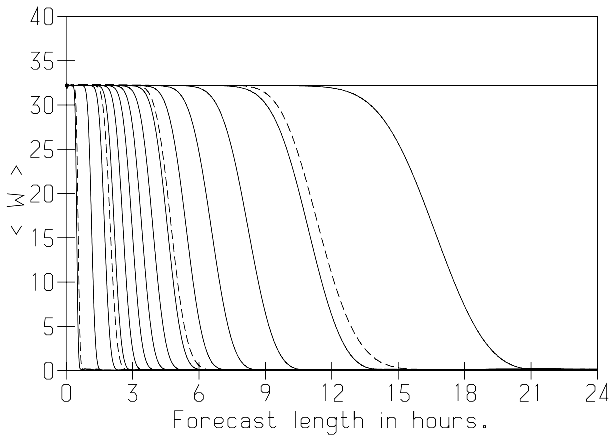

Fig. 1. The rms magnitude of each wave amplitude. The solid lines: positive velocity waves. The dashed lines: negative velocity waves.

$W_j = 0$ except for $j = m$, $\Psi_k^{(m)} = Q_{km} W_m$ defines the fields p_k, $k = 1, M$, and u_{k-M}, $k = M + 1, 2M$, for such a wave. To give each wave the same amplitude, put $W_m = W$. To guarantee that each field had approximately the same physical magnitude, the eigenvectors were normalized to 1:

$$\sum_{k=1}^{M} \Psi_k^{(m)} \Psi_k^{(m)} = W^2 \sum_{k=1}^{M} Q_{km} Q_{km} = W^2. \quad (40)$$

Thus, the initial state was given by

$$\Psi_k = W \sum_{m=1}^{M} Q_{km}. \quad (41)$$

The amplitude W was chosen so that the maximum value of $|u'_i(x, 0)|$, the physical wind anomaly, equals $10\,\mathrm{m\,s^{-1}}$ (Recall that $\rho_i^0 u'_i = u_i = \Psi_{i+M}$). The maximum anomaly for the other fields were also physically reasonable, 717 Pa for the pressure, $0.089\,\mathrm{kg\,L^{-1}}$ for density (equivalent to 17 K for temperature). In the x-direction, the fields were bell-shaped with a width of $L/10$ and centred at $L/2$.

The purpose of the test is to show that the boundaries are transparent to outgoing waves: the incoming waves have zero amplitude at the boundaries. Thus, in eq. (39), $W_m^r(0, t) = 0, m = 1, 15$; and $W_m^r(L, t) = 0, m = 16, 20$. All the other boundary wave amplitudes were built from the internal fields, by extrapolation as described in the appendix of McDonald (2005).

The forecast was run for 24 h. By that time, all the waves had exited the integration region except numbers 15 and 16, whose velocities are $3.8\,\mathrm{m\,s^{-1}}$ (328 km per 24 h) and $-2.9\,\mathrm{m\,s^{-1}}$ (-251 km per 24 h).

To illustrate how well the waves exit the integration region, the root mean square (rms) size of the 20 wave amplitudes W_m^n was computed at each time step n,

$$\langle W_m^n \rangle = \left[\sum_{i=1}^{I} \left\{ W_m^n(i) \right\}^2 \right]^{\frac{1}{2}} \quad (42)$$

and graphed. The result is shown in Fig. 1. Each wave can be seen exiting with almost no reflection, except for waves 15 and 16, which have not yet left the area after 24 h and are shown as constant lines. To get an accurate measure of the error, the rms difference between the fields u^n and $(u^h)^n$ was computed at each time step n. To measure the relative magnitude of this error, it was divided by the rms difference between the $(u^h)^n$ and zero at the start of the integration (time zero):

$$R^n(u) = \left[\sum_{i=1}^{I} \sum_{k=1}^{M} \{(u^h)_{i,k}^n - u_{i,k}^n\}^2 \right]^{\frac{1}{2}} \div \left[\sum_{i=1}^{I} \sum_{k=1}^{M} \{(u^h)_{i,k}^0\}^2 \right]^{\frac{1}{2}}. \quad (43)$$

The maximum value of $R^n(u)$ throughout the integration was 0.0068, confirming the picture painted by Fig. 1.

McDonald (2004), in tests involving the full primitive equations, used a constant advecting velocity to construct his transparent boundary conditions (because no other option was available). This prompts the question: how erroneous was that assumption, potentially? An indication can be obtained by repeating the above experiment, but now building new boundary fields, assuming a 'constant' advecting velocity, that is, $u^0(z)$ now equals $\bar{u}^0$. This involves two changes to the implementation of eqs. (37)–(39). First, instead of the matrices $\mathbf{Q}$ and $\mathbf{Q}^{-1}$ that diagonalize $\mathbf{A}$, those formally defined by eqs. (3.39) and (3.40) of McDonald (2005), with $\mathbf{E}$ being the set of eigenvectors that diagonalize $\mathbf{M}$ of eq. (31), were used. Second, the velocities $\bar{u}^0 \pm c_i$, $i = 1, M$ incoming or outgoing were used to distinguish the imposed from the extrapolated boundary fields. Here $\bar{u}^0 = \sum_{k=1}^{M} u_k^0 / M$ and c_i^2 are the eigenvalues of $\mathbf{M}$ defined in eq. (31). For the parameters defined above $\bar{u}^0 = 27.1\,\mathrm{m\,s^{-1}}$ and $\bar{u}^0 \pm c_i = 308.6$, 127.6, 81.7, 63.1, 52.5, 45.3, 40.0, 35.7, 32.0, 28.7, 25.4, 22.1, 18.4, 14.2, 8.8, 1.6, −9.0, −27.6, −73.4, −254.4, all of these having units of $\mathrm{m\,s^{-1}}$. Of these velocities, 16 are greater than and 4 are less than zero. Thus, not only will the matrices $\mathbf{Q}$ and $\mathbf{Q}^{-1}$ be inaccurate, but also one field too many will be imposed on the boundary in implementing eqs. (37)–(39).

Repeating the experiment with these 'no-shear' boundary conditions showed that the boundaries were no longer transparent: the maximum value of $R^n(u)$ throughout the integration was 0.28. The principal culprits were waves 12–14, which when they reached the $x = L$ boundary, were reflected mainly as projections onto waves 17–19. (Waves 15 and 16 did not reach the boundary).

3. Conclusions

A solution to the problem of how to adapt the so-called transparent boundary conditions to the physical reality that the horizontal advection velocity varies in the vertical, has been presented, and simple tests have demonstrated the new boundary conditions to be accurate.

The principal difference from the 'no-shear' derivation is that the system of equations no longer projects out as a set of M shallow water equations, as can be seen from eq. (29) (If u^0 is constant in the vertical, then $\mathbf{J} = \mathbf{K} = u^0\mathbf{I}$, and diagonalizing $\mathbf{M}$ yields M shallow water equations). This will complicate any implementation in a full non-linear three-dimensional system of equations.

It is not guaranteed that the matrix $\mathbf{A}$ has real eigenvalues. In fact, once the vertical shear is large enough, they become complex. The issue of boundary conditions for breaking waves was not addressed. To avoid inadvertently generating such a physical instability, the computer program had a 'stop' instruction if the matrix solver returned a complex eigenvalue for $\mathbf{A}$.

4. Acknowledgments

The helpful criticism of two anonymous reviewers is much appreciated.

References

Gill, A. E. 1982. In: *Atmosphere-Ocean Dynamics*. Academic Press, 662 pp.

McDonald, A. 2004. Transparent lateral boundary conditions for HIRLAM. The final shallow water tests and a first multi-level implementation. *HIRLAM technical report no. 62*, 26 pp.

McDonald, A. 2005. Transparent lateral boundary conditions for baroclinic waves: a study of two elementary systems of equations. *Tellus* **57A**, 171–182.

McDonald, A. 2006. Transparent lateral boundary conditions for baroclinic waves II. Introducing potential vorticity waves. *Tellus* **58A**, 210–220.